MICROSTRUCTURE AND PROPERTY MODIFICATIONS IN SURFACE LAYERS OF A AA6111 ALUMINUM ALLOY INDUCED BY HIGH-CURRENT PULSED RELATIVISTIC ELECTRON BEAM

D.E. Myla[1,2], V.V. Bryukhovetsky[1], V.V. Lytvynenko[1], S.I. Petrushenko[2], O.O. Nevgasimov[2], Yu.F. Lonin[3], A.G. Ponomarev[3], V.T. Uvarov[3]
[1]Institute of Electrophysics and Radiating Technologies NAS of Ukraine, Kharkiv, Ukraine
E-mail: ntcefo@yahoo.com;
[2]V.N. Karazin Kharkiv National University, Kharkiv, Ukraine
E-mail: postmaster@univer.kharkov.ua;
[3]NSC "Kharkov Institute of Physics and Technology", Kharkiv, Ukraine
E-mail: nsc@kipt.kharkov.ua

The processing of the AA6111-T4 aluminum alloy by the high-current relativistic electron beams affects the forming of the surface layer with a modified structure and phase state. The depth of the modified surface layer achieves 200 μm. The changes in microstructure occurring both in the near-surface layer and in the modified layer can be distinguished with XDR, SEM, and EDS analyses. It is established that the aluminum-based supersaturated solid solution makes the main phase of the modified layer, whereas intermetallic phases that were present in the initial state of the alloy are not distinguished by the X-ray methods in the modified layer. There are some available microcracks and craters on the surface of the remelt layer. Discussion of the results of these observations gains a more sufficient understanding of the processes raised by the irradiation by a high-current relativistic electron beam.

INTRODUCTION

The trends to create new material with modified surface layer properties meet the basic requirements of modern science and technology. That is the reason for conducting a great deal of research to study the influence of the intense energy fluxes on the surface properties of solid bodies. This method causes no changes of the inner layers of the treated materials that could change the surface properties i.e. structure, microhardness, wear resistance, corrosion resistance in a targeted manner. The intense energy fluxes employ shock and electromagnetic waves, plasma jets, laser radiation, as well as ionic fluxes, and electron beams. The latest trend reveals that the intense pulsed electron beam is gaining more and more attention in the field of surface treatment employing various energy and time beam parameters [1−10]. One of the main factors of such influence is a heating effect connected with the liquation of the surface layer of the metal. Whereas the ultrarapid quenching of the liquid phase metal surface allows forming of nonequilibrium structure and phase states in the surface layer within unsteady temperature fields and thermal stress. Analysis of the already existing fundamentals and experimental materials shows that in a short period of time under the effect of intense pulsed electron beam radiation the material comes through a lot of processes: ultrarapid heat gain, material evaporation, phase transformations, irritation of acoustic and shock waves, surface hardening, etc. However, the physical essence of the above-mentioned processes is understudied, preventing the complete understanding of their mechanisms and behavior.

In this article, we investigate AA6111 aluminum alloy launched by Alcan Company in 1983 [11]. This alloy belongs to the wide range of the heat-treatable aluminum alloys of the Al-Mg-Si ternary system. These alloys come along with improved workability, corrosion resistance, rather a high ductility so they are applied in automotive, construction, as well as space, and aircraft industries. The AA6111 sheets are widely used for the production of vehicle bodies [12]. The properties of the heat-treatable aluminum alloys sufficiently depend on the cooling rate of the semi-finished product at the quenching step establishing the structure and rate of the residual stresses. Surface properties become excessively important ones for this alloy as the vehicle bodies shall meet improved hardness and extreme corrosion resistance. The target of this research is to investigate the structure and phase state, microhardness, and the compound of the upper surface layer, and a near-surface layer of the AA6111 aluminum alloy after its processing by a highly-current relativistic electron beam.

EXPERIMENTAL PROCEDURE

Irradiation of alloy sheets was performed by a high-current pulsed relativistic electron beam (HCPREB) at the TEMP-A accelerator in the NSC KIPT of the NAS of Ukraine [1, 5, 9]. The energy flux density at the W target is approximately $10^9 W/cm^2$ (beam energy is E ~ 0.35 MeV, current is I ~ 2000 A, pulse duration is τ_i ~5·10^{-6} s, beam diameter is D ~ 3 cm). Irradiation was produced by a single impulse in a vacuum at 1.3·10^{-3} Pa.

The microstructure was studied using a SEM Tescan VEGA 3 LMH, a scanning electron microscope. The Vickers microhardness was measured at room temperature in air using the PMT-3 microhardness tester. Microhardness tested with load of 50g and load duration of 25 s. The qualitative and quantitative X-ray

analyses were performed on a Shimadzu XRD-6100 X-ray diffractometer. The energy dispersive X-ray microanalysis of the local microvolumes of the irradiated alloy layers was performed using a SEM Tescan VEGA 3 LMH, a scanning electron microscope with the Bruker XFlash 5010 SSD EDS detector.

The distribution of the alloying elements along the polished specimen surface was distinguished in the mapping mode with a SEM of Tescan VEGA 3 LMH and the method of EDS analysis.

RESULTS AND DISCUSSION

The material investigated in this study was a commercial AA6111-T4 aluminum alloy, with the chemical composition listed in Table 1. T4 – solution heat-treated and naturally aged. Despite the basic alloying elements (Si and Mg) providing with the order and precipitation hardening the alloys of 6xxx grade can be alloyed with copper (to improve the physical characteristics), chromium (to compensate for the negative impact of copper affecting the corrosion resistance), and manganese, the last two elements prevent the silicon segregation along the grain boundaries [12].

Table 1

Chemical composition (wt.%)
of AA6111 aluminum alloy

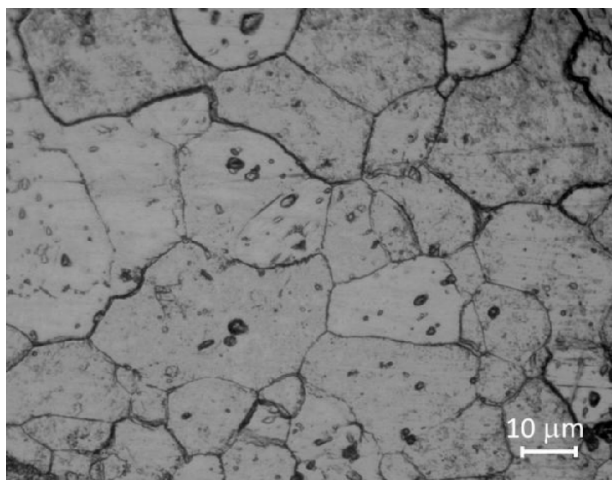| Mg	Si	Cu	Mn	Fe	Cr	Al
0.5-0.9	0.7-1.1	0.5-0.7	0.1-0.4	0.1-0.4	0.1	Bal.

Fig. 1. Optical microscopy micrographs of initial AA6111 alloy

Fig. 1 shows initial microstructure of the AA6111-T4 aluminum alloy. The AA6111-T4 average grain size was distinguished as one equal to 40 μm. The grains come in different sizes but there is no open metallographic structure. Destructive testing of AA6111-T4 alloy specimen at the room temperature allowed finding out, that its tensile strength made $\sigma_{tensile}$ = 340 MPa, while yield strength made σ_{yield} = 152 MPa. Ultimate tensile strength before breaking of AA6111-T4 at room temperature made 21%. Microhardness of AA6111-T4 alloy made $70HV0.50$. The alloy showed superplastic behavior despite its large grain sizes [13, 14]. At the temperature equal to T = 793 K and the true deformation rate equal

to $\dot{\varepsilon}$ = 5,2·10^{-4} c^{-1} the alloy tensile strength before breaking made 180%.

For further irradiation we cut a 100×100 mm specimen out of AA6111-T4 sheet of 1.1 mm thickness. The SEM micrographs in Fig. 2,a show the area of the specimen surface of AA6111-T4 alloy irradiated by HCPREB. The HCPREB irradiation (with the established beam parameters in the paper) causes flash heating rate up to 10^9 K/s, achieving the high temperature that dramatically exceeded the critical melt temperature of the aluminum alloy [9]. Under the HCPREB treatment the alloy heating rate is higher in the deeper surface layers. The maximum energy absorption occurs at a depth of approximately 1/3 of the electron path in the alloy. It causes the explosion of some remelted material with further rapid cooling and the corresponding heat transfer to the host alloy. Such cooling is accompanied by crystallization of the molten material, causing structural and phase transformations.
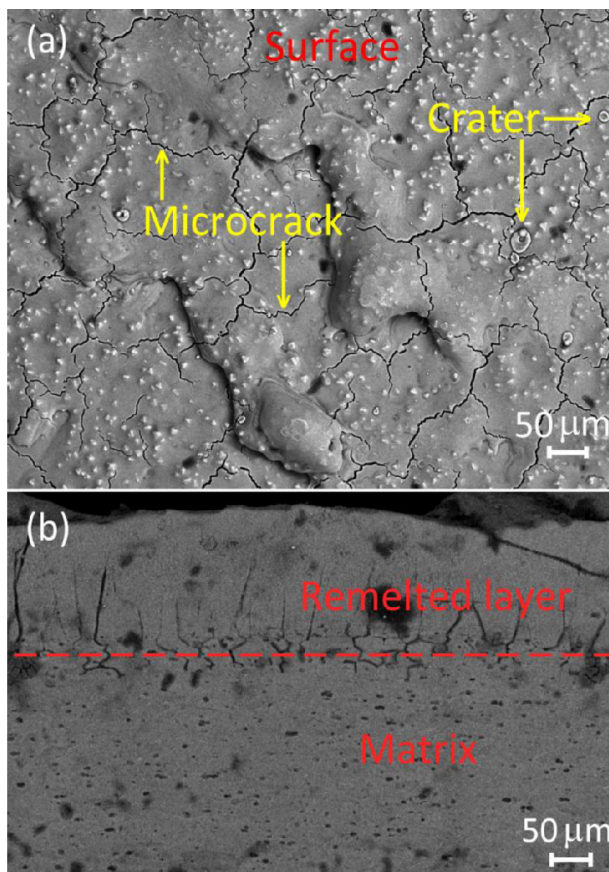

Fig. 2. SEM image of the irradiated surface of AA6111-T4 alloy (a); SEM image of the alloy cross-section in the zone of electron beam irradiation (b)

The thickness of the molten layer (see Fig. 2,b) makes 200 μm. There are some microcracks and craters on the surface (see Fig. 2,a). Fig. 2,b exhibits the microcrack behavior propagating along the whole depth of the remelt surface layer. The zig-zag pattern of the microcrack distribution along the surface may be related to the local inhomogeneity distribution of the alloying elements in the solidified substance and with local inhomogeneity of the strength and ductile properties of the solidified substance in its various micro volumes.

The availability of such surface microcracks is a typical appearance of the aluminum alloys irradiated by HCPREB [1, 3, 7, 9]. A lot of scientists [6] observe craters and consider them as the most abundant feature we can find on the surface of the metallic substances irritated by HCPREB. The main assumptions explaining the ways of crater propagating are: inhomogeneous local melting in the near-surface layer of the host alloy in the zones of low-melting point eutectic concentration; projections on a rough surface, closing channels with high current density; the presence of the beam filamentary inclusions of high current density and the consequent eruption of molten material towards the beam effect [6].
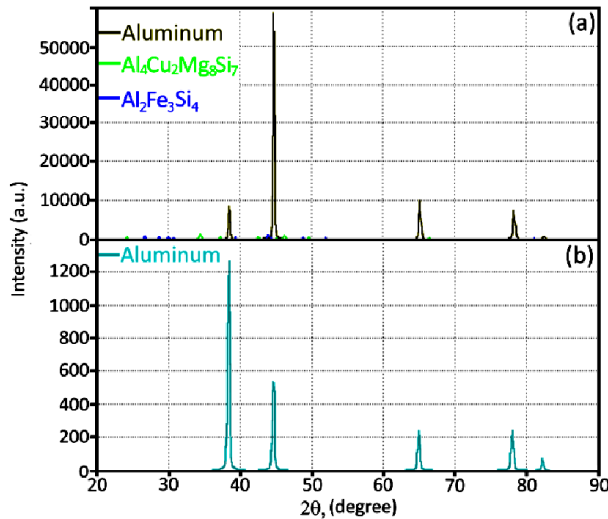

Fig. 3. XRD patterns of AA6111-T4 aluminum alloy before (a) and after (b) HCPREB irradiation
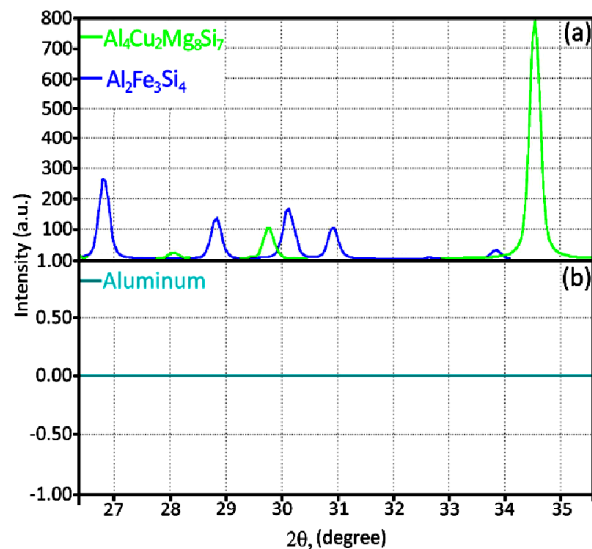

Fig. 4. A part of scaled-up XRD patterns of AA6111-T4 aluminum alloy before (a) and after (b) HCPREB irradiation

Fig. 3 shows the XRD patterns of AA6111-T4 aluminum alloy before and after HCPEB irradiation. Fig. 4 shows the part of the scaled-up XRD patterns of AA6111 aluminum alloy before and after HCPEB irradiation. Thus we can see that the highest XRD peaks correspond to the solid aluminum-based solution phase

(α_{Al}-phase). The XRD pattern of the AA6111-T4 alloy specimen before irradiation shows the typical phase peaks of $Al_2Fe_3Si_4$ (33.3 Fe, 44.4 Si, at.%), and $Al_4Cu_2Mg_8Si_7$ (9.5 Cu, 38.1 Mg, 33.3 Si, at.%). Whereas the XRD pattern of the AA6111-T4 alloy specimen after irradiation comes without the $Al_2Fe_3Si_4$ phase and without $Al_4Cu_2Mg_8Si_7$ phase. Thus, we can come to the conclusion that either the above phases have completely been dissolved in the aluminum matrix at the irradiating by HCPREB or there are only their insufficient traces. The comparison of Fig. 3,a,b XRD patterns confirms that the irradiation affects the redistribution of the crystal orientation of the aluminum-based solid solution due to the change in the peak intensity ratio in XRD patterns for α_{Al}-phase. Herewith we can see a descending trend for α_{Al}-phase peak intensity ratio in the irradiated layer. It makes [200] to [111]. Moreover the irradiation by HCPREB shows the trend to extend the α_{Al}-phase peak width. The obvious widening trend of the Bragg reflection can be related to the grain size reduction and the trace inner stress increase. The α_{Al}-phase peaks of the irradiated layer in Fig. 3 are dislocated towards the smaller angles confirming the increase of the lattice parameter. It is established that the lattice parameter in the irradiated surface layer makes 0.405327 nm, whereas the as-cast target AA6111-T4 alloy had the lattice parameter equal to 0.404528 nm.

The SEM analysis shows the visible intermetallic particles and their distribution along the as-cast, before the irradiation sheet of the AA6111-T4 alloy (Fig. 5). The specimen in Fig. 5,a has not been polished. We can see the intermetallic particles of rough shape and that they are distributed inhomogonicaly. The sizes of some particles exceed 10 μm. The SEM image (see Fig. 5,b) shows the ground and polished surface of the AA611-T4 alloy specimen. The dark spots in Fig. 5,b reveal some cavities propagated at the specimen processing (grinding and polishing): any mechanical treatment of the specimen surface *i.e.* friction makes some solid particles get separated out of the soft aluminum matrix leaving the cavities on the surface.

Fig. 5,b shows the zones subjected to be tested by EDS analyses. The zones were selected randomly. You can check Table 2 for the as-cast chemical compound of the selected zone of AA6111-T4 (before the irradiation by HCPREB). Every single value in Table 2 is actually an average value for the randomly selected zones. Please note, that the provided T4 treatment of the as-cast AA6111 alloy involved quenching in order to obtain the best concentration of the alloying elements (basically of Mg, Si and Cu) in the aluminum-based solid solution and provide with extremely hardening effect at the further ageing. The majority of the coarse intermetallic particles was ground and polished away off the surface (see Fig. 5,b). Therefore, we can consider that the data in Table 2 shows the quantity of the alloying elements available in the aluminum-based solid solution of the initial AA6111-T4 alloy specimen before irradiation step.
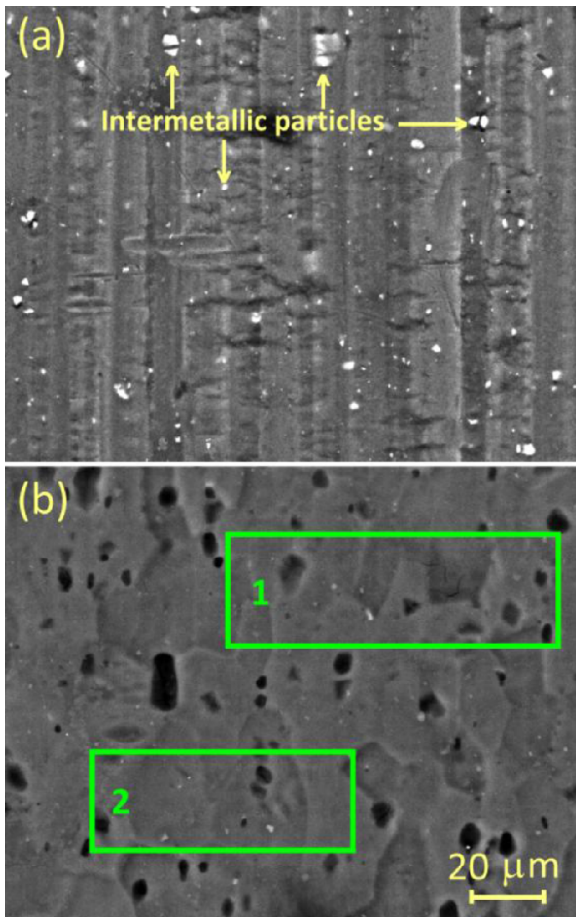
Fig. 5. SEM image of intermetallic particles on the surface of the AA6111 aluminum alloy: a – surface before grinding and polishing; b – surface after grinding and polishing. Zone 1 and 2 in Fig. 5,b are the schematic dislocation of the zone to be tested by EDS

Table 2

EDS analysis results of zones 1 and 2 in Fig. 5,b

Spectrum	Mg	Al	Si	Mn	Fe	Cu
1	0.85	98.71	0.13	0.03	0.07	0.21
2	0.79	98.84	0.11	0.02	0.06	0.18

After studying the data in Table 2 we can confirm that almost all magnesium and the considerate share of copper are distributed in the aluminum-based solid solution. Although silicon dissolution in aluminum at room temperature is not high, some quantities of silicon have moved into aluminum-based solid solution.

Fig. 6 shows EDS elemental maps for the specimen alloy before irradiation by HCPREB. These images reveal intentionally increased contrast levels in order to better display the difference in chemical composition between the different types of precipitates present in the microstructure. We can see that the Si particle availability is typical for the structure state of the AA6111-T4 alloy. The coarse Si particle diameter can achieve 30 μm, the distribution of these particles along the specimen treated surface is inhomogeneous. We can explain the availability of the rather coarse Si particles in the AA6111-T4 alloy: at room temperature the dissolving ability of silicon in aluminum is rather high (0.09% at 300 °C). If the iron content in the alloy exceeds the silicon content, the silicon performs ternary

compounds of $Al_xFe_xSi_x$. The availability of magnesium in Al-Si alloy leads to the propagating of the fine Mg_2Si particles. XRD analysis did not confirm the availability of Mg_2Si phase in the investigated alloy but it confirmed the sufficient quantity of silicon exceeding the iron quantity. Therefore, despite the existence of $Al_2Fe_3Si_4$ phase existence with its crystalline origin, some quantities of silicon are present in the shape of coarse particles that were distinguished in the EDS elemental maps. We have to admit that XRD analyses did not find the phase of the pure silicon. We can explain this with the fact that the silicon particles in the initial AA6111-T4 specimens (before irradiation) are rather coarse ones and distributed inhomogeneously.
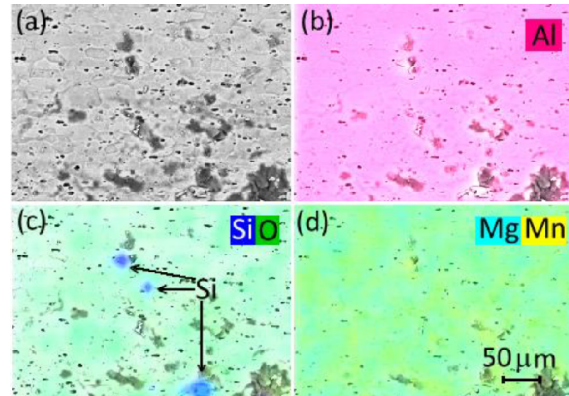

Fig. 6. EDS maps of the Si particles in the AA6111 alloy revealing the elemental distribution of Mg, Cu, Si, Al

Fig. 7 reveals the cross-section of the specimen in the zone irradiated by the electron beam. Fig. 7,a shows the zones of EDS investigations. These zones were selected randomly both for the base metal and for the surface layer remelted by electron beam. You can find their chemical compounds in Table 3. Every single value in Table 3 is an average value for the randomly selected zones. The chemical compound is one of the basic features of the metal structure after irradiation by HCPREB. Table 3 data analyses and the data comparison with the ones in Table 2 allow us to make the following conclusions concerning the redistribution of the alloying elements in the aluminum-based solid solution after irradiation by HCPREB. First of all we can notice the fact of the reduced quantities of Mg atoms in the surface layer after irradiation. It might occur due to the reason that the heated in vacuum alloy surface is depleted with more volatile constituents including Mg. But there is a reverse trend for the atoms of Si, Cu, Fe, and Mn, their quantities are accumulating in the irradiated by HCPREB zones. The reason for such a behavior is the partial or complete dissolution or melting, and further distribution in the molt of available intermetallic phases in the initial alloy state. Thus, a new aluminum-based solid solution propagates in the remelted layer after irradiation by HCPREB. However we should consider the fact of significant increase of Si atom quantitates in the new solid solution. The reason for such an increase can occur due to the melt of the coarse silicon particles at the irradiation by HCPREB. The melting temperature of silicon is 1688 K. It is rather high temperature so there is a probability that silicon

particles will not melt at the irradiation by HCPREB. However the partial or even complete melting of silicon particles (it depends on the particle size) can occur in compliance with the contact melting method [15–17]. The effect of the impact fusion method occurs along $L \leftrightarrow \alpha_{Al} + Si$ the boundary between the aluminum based solid solution and silicon particle at the temperature of 850 K. At this temperature the maximal dissolutive ability of silicon in aluminum makes 1.65% [18].
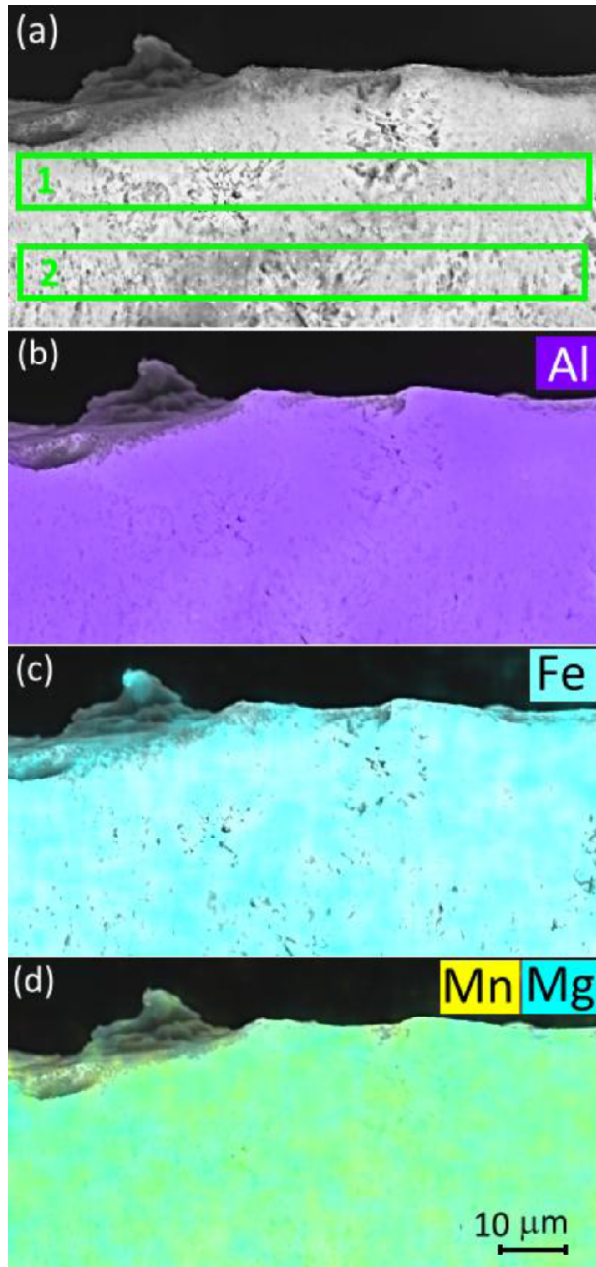

Fig. 7. The EDS elemental maps of the cross-section of the remelted layer of AA6111-T4 alloy

Fig. 7,b–d reveals the research results of the Al, Fe, Mn, and Mg atom distribution along the cross-section of the remelted layer performed in the mapping mode. We can observe homogeneous behaviour of the distribution of these atoms along the cross-section. This homogeneous distribution of the alloying elements can confirm the homogeneity of physical and mechanical properties of the AA6111-T4 alloy remelted layer by HCPREB irradiation.

Table 3
EDS analysis results of the zones selected in Fig. 7,a

Spectrum	Mg	Al	Si	Mn	Fe	Cu
1	0.61	98.53	0.37	0.07	0.11	0.31
2	0.57	98.56	0.41	0.05	0.13	0.28

The structure state and phase transformations in the investigated alloy affected by the HCPREB irradiation should lead to the changes of the alloy strength properties *i.e.* mainly to microhardness. We established the microhardness value of the layer after irradiation by HCPEB- it was $101HV0.50$. Based on the knowing microhardness we can assume other mechanical properties of the alloy. There are some methods to identify the yield strength and tensile strength limits based on the microhardness value. In compliance with [19] the Vickers microhardness (HV) is an equivalent to the true stress at the 8% deformation and could be found in Equation 1:

$$\sigma_8 (MPa) = 3.27 HV . \tag{1}$$

If to apply to the Al-Mg-Si ternary system we can perform the conversion from yield strength (in MPa) to hardness HV (in VPN) via a simple regression equation [20]:

$$\sigma_y = \frac{HV - 16.0}{0.33} . \tag{2}$$

According to Equation (2) the microhardness of the modified layer equal to $101HV0.50$ should correspond to the $\sigma_{0.2}$ value approximately equal to 257 MPa. Thus, we can stipulate that the yield strength of the modified layer by the HCPREB irradiation increases over 100 MPa. It is known that precipitation age hardening is the basic mechanism to improve the hardening of the alloy of 6xxx grade [21]. The best mechanical properties are achieved by employing T6 treatment including quenching and consequent aging [22]. The hardening of this system alloys is mostly related to propagation of fine Mg_2Si phase emission at the aging step [21–23]. We assume that the irradiation by HCPREB affects the hardening of AA6111-T4, by the refining of the grain sizes, improving their dislocation density as well as by the accumulation of the silicon and copper quantities in the aluminum-based solid solution. Please note, that the work [22] assures that the maximal value of the yield strength of the AA6111 alloy equal to 340 MPa was achieved after 7 h of the aging process at the temperature of 180 °C. Thus, for the dispersion hardening of the alloy we should employ rather long treatment whilst the the HCPEB irradiation leads to the significant hardening in a short period of time with a prospective probability of the further increase strengths due to the propagating of Mg_2Si particles or clusters of the dissolved atoms [24] if the substance is operating in high temperatures.

CONCLUSIONS

1. The irradiation by pulsed electron beam affecting the AA6111-T4 alloy specimen leads to the melt of the surface layer at the depth of 200 μm. The surface of the remelted layer reveals microcrack and crater patterns propagating at the crystallization.

2. XRD pattern of the AA6111-T4 alloy specimen shows peaks of $Al_2Fe_3Si_4$ phase and $Al_4Cu_2Mg_8Si_7$ phase, these peaks are typical for the surface before irradiation by HCPREB, and they are not available in the XRD pattern of the specimen after the irradiation by HCPREB. We assume that either these phases were completely dissolved in the aluminum matrix at the HCPREB irradiation or there are available only their insufficient traces in the irradiated layer. The irradiation leads to the redistribution of the crystal orientation of the aluminum-based solid solution.

3. After irradiation by HCPREB a new aluminum-based solid solution is propagated in the remelted layer. The quantities of the Mg atoms are reduced whereas the Si, Ci, Fe, and Mn atom quantities have the reverse trend − they are accumulated in the aluminum-bases solid solution layer after irradiation by HCPREB. These transformations are performed due to the reason that the heated in vacuum alloy surface is depleted with more volatile constituents including Mg as well as the available intermetallic phases in the initial alloy state are partially or completely dissolved or melted, and then distributed in the molt.

4. The structure state and phase transformations in the alloy are caused by the HCPREB irradiation. It leads to the hardening of the surface layer of the AA6111-T4 alloy with improving of the yield strength more than 100 MPa. The hardening of the irradiated layer is performed due to the refining of the grain sizes, dislocation density increase and accumulating of the silicon and copper quantities in the aluminum-based solid solution.

REFERENCES

1. V.V. Bryukhovetsky, V.F. Klepikov, V.V. Lytvynenko, D.E. Myla, V.P. Poyda, A.V. Poyda, V.T. Uvarov, Yu.F. Lonin, A.G. Ponomarev. The features of the structural state and phase composition of the surface layer of aluminum alloy Al-Mg-Cu-Zn-Zr irradiated by the high current electron beam // *Nuclear Inst. and Methods in Physics Research B*. 2021, v. 499, p. 25-31.

2. Y. Hao, B. Gao, G.F. Tu , S.W. Li , C. Dong, Z.G. Zhang / Improved wear resistance of Al–15Si alloy with a high current pulsed electron beam treatment // *Nuclear Inst. and Methods in Physics Research B*. 2011, v. 269, p. 1499-1505.

3. D.E. Myla, V.V. Bryukhovetsky, V.V. Lytvynenko, V.P. Poyda, A.V. Poyda, V.F. Klepikov, V.T. Uvarov, Yu.F. Lonin, A.G. Ponomarev // Analysis of changes in the phase and structural state of the surface layer of an aluminum alloy 1933, melted by a pulsed electron beam // *Problems of Atomic Science and Technology*. 2020, N 2(126), p. 33-38.

4. D.V. Zaguliaev, Yu.F. Ivanov, A.A. Klopotov, A.M. Ustinov, V.V. Shlyarov, D.F. Yakupov. Evolution of strength properties and defect sub-structure of the hypoeutectic A319.0 alloy irradiated by a pulsed electron beam and fractured under tensile stress // *Materialia*. 2021, v. 20, p. 101223; https://doi.org/10.1016/j.mtla.2021.101223

5. V.T. Uvarov, V.V. Uvarov, V.N. Robuk, N.I. Bazaleev, A.G. Ponomarev, A.N. Nikitin, Yu.F. Lonin, T.I. Ivankina, V.F. Klepikov, V.V. Lytvynenko, S.Ye. Donets. Radiation acoustic control over the thermal parameter of construction materials irradiated by intense relativistic electron beam // *Phys. of Part. and Nucl. Latter*. 2014, v. 11, N 3, p. 274-281.

6. D.I. Proskurovsky, V.P. Rotshtein, G.E. Ozur, Y.F. Ivanov, A.B. Markov. Physical foundations for surface treatment of materials with low energy, high current electron beams // *Surface and Coatings Technology*. 2000, v. 125, N 1-3, p. 49-56.

7. V.V. Bryukhovetsky, A.V. Poyda, V.P. Poyda, D.E. Milaya, Superplastic deformation of the AK4-1 alloy with a surface layer melted by electron pulse beam // *Problems of Atomic Science and Technology*. 2019, N 2(120), p. 67-73.

8. V.V. Bryukhovetskiy, N.I. Bazaleev, V.F. Klepikov, V.V. Litvinenko, O.E. Bryukhovetskay, E.M. Prokhorenko, V.T. Uvarov, A.G. Ponomar'ov. Features of gelation of surface of industrial aluminium alloy 6111 in the area of influence of impulsive bunch of electrons in the mode of pre-melting // *Problems of Atomic Science and Technology*. 2011, N 2(72), p. 28-32.

9. A.G. Kobets, P.R. Horodek, Yu.F. Lonin, V.V. Lytvynenko, A.G. Ponomarev, O.A. Startsev, V.T. Uvarov. Melting effect on high current electron beam on aluminum alloy 1933 // *Surface Engineering and Applied Electrochemistry*. 2015, v. 51, N 5, p. 478-482.

10 V.V. Bryukhovetskii, V.V. Litvinenko, V.F. Klepikov, R.I. Kuznetsova, V.P. Poida, V.F. Kivshik, and V.T. Uvarov. Effect of Pulse Electron Irradiation on the Parameters of Duralumin Superplasticity // *Fiz. Khim. Obrab. Mater*. 2002, N 4, p. 33-38 (in Russian).

11. P.E. Fortin, M.J. Bull, and D.M. Moore. *SAE Int. Congr. Exp.*, Detroit, MI, 1983, SAE Paper no. 830096.

12. P. Mukhopadhyay. Alloy Designation, Processing, and Use of AA6XXX Series Aluminium Alloys // *ISRN Metallurgy*. 2012, v. 2012, Article ID 165082, p. 1-15.

13. V.V. Bryukhovetskyy, V.P. Pojda, A.V. Poyda, D.R. Avramets', R.I. Kuznetsova, O.P. Kryshtal', O.L. Samsonnik, K.A. Mahmud. Mechanical properties and structural changes during superplastic deformation of 6111 aluminium alloy // *Metallofiz. Noveishie Tekhnol*. 2009, v. 31, issue 9, p. 1289-1302 (in Russian).

14. V.V. Bryukhovetskij. On the origin of high-temperature superplasticity of a coarse-grained avial-type aluminum alloy // *Fizika Metallov i Metallovedenie*. 2001, v. 92, issue 1, p. 107-111 (in Russian)

15. V.V. Bryukhovetsky, R.I. Kuznetsova, N.N. Zhukov, V.P. Poida, V.F. Klepikov. Liquid-phase nucleation and evolution as a cause of superplasticity in alloys of the Al-Ge system // *Phys. Stat. Sol. (A)*. 2005, v. 202, N 9, p. 1740-1750.

16. A.V. Pojda, V.V. Bryukhovets'ky, D.L. Voronov, R.I. Kuznetsova, V.F. Klepikov. Superplastic behaviour of an AlMg6 alloy at the high homological temperatures // *Metallofiz. Noveishie Tekhnol*. 2005, v. 27, issue 3, p. 317-330. (in Russian)

17.V.P. Poida, D.E. Pedun, V.V. Bryukhovetskii, A.V. Poida, R.V. Sukhov, A.L. Samsonik, V.V. Lit-

vinenko, Structural changes during superplastic deformation of high-strength alloy 1933 of the Al-Mg-Zn-Cu-Zr system // *Phys. Met. Metallogr.* 2013. v. 114, N 9, p. 779-788.

18. L.F. Mondolfo. *Aluminum Alloys: Structure and Properties.* London: "Butterworths", 1979, 513 p.

19. D. Tabor. Indentation Hardness: Fifty Years on. A Personal View // *Phil. Mag. A.* 1996, v. 74, N 5, p. 1207-1212.

20. O.R. Myhr, Ø. Grong, S.J. Andersen. Modelling of the age hardening behaviour of Al-Mg-Si alloys // *Acta Materialia.* 2001, v. 49, issue 1, p. 65-75.

21. C.D. Marioara, S.J. Andersen, H.W. Zandbergen, R. Holmestad. The influence of alloy composition on precipitates of the Al-Mg-Si system // *Metallurgical and Materials Transactions A.* 2005, v. 36, p. 691-702.

22. S. Esmaeili, X. Wang, D.J. Lloyd, W.J. Poole. On the precipitation-hardening behavior of the Al-Mg-Si-Cu alloy AA6111 // *Metall. Mater. Trans. A.* 2003, v. 34, p. 751-763.

23. X. Wang, S. Esmaeili, D.J. Lloyd. The sequence of precipitation in the Al-Mg-Si-Cu alloy AA6111 // *Metallurgical and materials transactions A.* 2006, v. 37, p. 2691-2699.

24. R.K.W. Marceau, A. de Vaucorbeil, G. Sha, S.P. Ringer, W.J. Poole. Analysis of strengthening in AA6111 during the early stages of aging: Atom probe tomography and yield stress modeling // *Acta Materialia.* 2013, v. 61, p. 7285-7303.

МОДИФІКАЦІЯ МІКРОСТРУКТУРИ І ВЛАСТИВОСТЕЙ ПОВЕРХНЕВИХ ШАРІВ АЛЮМІНІЄВОГО СПЛАВУ AA6111 ДІЄЮ ПОТУЖНОГО ІМПУЛЬСНОГО РЕЛЯТИВІСТСЬКОГО ЕЛЕКТРОННОГО ПУЧКА

Д.Є. Мила, В.В. Брюховецький, В.В. Литвиненко, С.І. Петрушенко, О.О. Невгасимов, Ю.Ф. Лонін, А.Г. Пономарьов, В.Т. Уваров

Обробка алюмінієвого сплаву AA6111-T4 інтенсивним імпульсним електронним пучком приводить до формування поверхневого шару з модифікованим структурно-фазовим станом. Глибина поверхневого модифікованого шару досягає 200 мкм. Зміни мікроструктури, що відбуваються в поверхневому шарі і на модифікованій поверхні, були охарактеризовані за допомогою рентгенівської дифрактометрії, електронної мікроскопії та рентгенівського енергодисперсійного мікроаналізу. Встановлено, що основною фазою модифікованого шару є пересичений твердий розчин на основі алюмінію, а інтерметалідні фази, які були присутні в початковому стані сплаву, рентгенографічними методами в модифікованому шарі не виявляються. На поверхні переплавленого шару присутні протяжні мікротріщини і кратери. Обговорюється значення цих спостережень для більш глибокого розуміння процесів, що відбуваються під час імпульсного електронного опромінення алюмінієвих сплавів.

МОДИФИКАЦИЯ МИКРОСТРУКТУРЫ И СВОЙСТВ ПОВЕРХНОСТНЫХ СЛОЕВ АЛЮМИНИЕВОГО СПЛАВА AA6111 ДЕЙСТВИЕМ СИЛЬНОТОЧНОГО ИМПУЛЬСНОГО РЕЛЯТИВИСТСКОГО ЭЛЕКТРОННОГО ПУЧКА

Д.Е. Милая, В.В. Брюховецкий, В.В. Литвиненко, С.И. Петрушенко, А.О. Невгасимов, Ю.Ф. Лонин, А.Г. Пономарев, В.Т. Уваров

Обработка алюминиевого сплава AA6111-T4 интенсивным импульсным электронным пучком приводит к формированию поверхностного слоя с модифицированным структурно-фазовым состоянием. Глубина поверхностного модифицированного слоя достигает 200 мкм. Изменения микроструктуры, происходящие в приповерхностном слое и на модифицированной поверхности, были охарактеризованы с помощью рентгеновской дифрактометрии, электронной микроскопии и рентгеновского энергодисперсионного микроанализа. Установлено, что основной фазой модифицированного слоя является пересыщенный твердый раствор на основе алюминия, а интерметаллидные фазы, которые присутствовали в исходном состоянии сплава, рентгенографическими методами в модифицированном слое не обнаруживаются. На поверхности переплавленного слоя присутствуют протяженные микротрещины и кратеры. Обсуждается значение этих наблюдений для более глубокого понимания процессов, происходящих во время импульсного электронного облучения алюминиевых сплавов.